



Research article

Modeling the effect of VOCs from biomass burning emissions on ozone pollution in upper Southeast Asia



Teerachai Amnuaylojaroen^{a,b,*}, Ronald C. Macatangay^c, Suratsawadee Khodmanee^a

^a Department of Environmental Science, School of Energy and Environment, University of Phayao, Phayao, 56000, Thailand

^b Atmospheric Pollution and Climate Change Research Unit, School of Energy and Environment, University of Phayao, Phayao, 56000, Thailand

^c Atmospheric Research Unit, National Astronomical Research Institute of Thailand, Chiang Mai, 53000, Thailand

ARTICLE INFO

Keywords:

Environmental science
Atmospheric science
Climatology
Environmental chemistry
Environmental pollution
Earth-surface processes
Volatile organic compounds
Surface ozone
WRF-CHEM model
Southeast Asia

ABSTRACT

We used a Weather Research and Forecasting Model with Chemistry (WRF-CHEM) model that includes anthropogenic emissions from EDGAR-HTAP, biomass burning from FINN, and biogenic emissions from MEGAN to investigate the main volatile organic compound (VOC) ozone precursors during high levels of biomass burning emissions in March 2014 over upper Southeast Asia. A comparison between the model and ground-based measurement data shows that the WRF-CHEM model simulates the precipitation and 2 m temperature reasonably well, with index of agreement (IOA) values ranging from 0.76 to 0.78. Further, the model predicts O₃, NO₂, and CO fairly well, with IOA values ranging from 0.50 to 0.57. However, the magnitude of the simulated NO₂ concentration was generally underestimated compared to OMI satellite observations. The model result shows that CO and VOCs such as BIGENE play an important role in atmospheric oxidation to surface O₃. In addition, biomass burning emissions are responsible for increasing surface O₃ by ~1 ppmv and increasing the reaction rate of CO and BIGENE by approximately 0.5×10^6 and 1×10^6 molecules/cm³/s, respectively, in upper Southeast Asia.

1. Introduction

O₃ is a major air pollutant that can have negative effects on human health, agriculture, weather, and climate (Nuvolone et al., 2018; Felzer et al., 2007; Ebi and McGregor, 2008). For example, Bell et al. (2004) and Bell and Dominici (2008), who investigated the health effects of O₃ exposure in the United States in 1987–2000, found that a 10 ppbv increase in ozone was associated with a 0.52% increase in mortality and a 0.64% increase in cardiovascular and respiratory mortality. Recent calculations of global premature mortality rates based on high-resolution global model simulations of O₃ and PM_{2.5} revealed that Southeast Asia and the Western Pacific have the highest premature mortality rates worldwide, which account for approximately 25% and 45% of the global mortality rate in 2005, respectively (Lelieveld et al., 2013). The total number of regional premature deaths from anthropogenic ozone is estimated to be approximately 33,300 in Southeast Asia (Lelieveld et al., 2013). The effect of O₃ on the agricultural ecosystem was reviewed by Lenka and Lenka (2012), who presented evidence of a reduction in crop yields due to increasing levels of O₃ and suggested that this effect may partially explain the decline in crop yields in South Asia. As reported by Amnuaylojaroen et al. (2018), with changes in the climate and emissions,

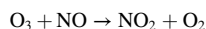
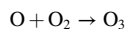
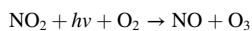
the O₃ levels over Southeast Asia will tend to increase by 10%–27% in the future. In addition, O₃ also plays a central role in tropospheric chemistry as a precursor of the hydroxyl (OH) radical, which acts as a detergent in the atmosphere. Therefore, it is very important to understand the processes controlling the formation and distribution of O₃.

O₃ is not directly emitted by anthropogenic or natural sources, but instead is the product of photochemistry between volatile organic compounds (VOCs), nitrogen oxides (NO_x = NO + NO₂), and carbon monoxide (CO). Though often present at levels of only 1 ppb or less, nitrogen oxides play a central role in the chemistry of the troposphere (Melkonyan and Kuttler, 2012). The gas-phase chemistry of the troposphere involves the oxidation of organic molecules in the presence of nitrogen oxides under the influence of sunlight. Atmospheric oxidation proceeds via chains of free radical reactions. Because atmospheric oxidation involves a very dilute fuel, at mixing ratios of parts per million or even parts per billion, an external source of energy is required to drive the reactions, and that energy is provided by solar radiation (Seinfeld and Pandis, 1998). In the urban and continental troposphere, many other anthropogenic and biogenic hydrocarbons and organic species are present. As a result of combustion emissions, greatly enhanced levels of NO_x over those in the background troposphere exist in urban and continental areas,

* Corresponding author.

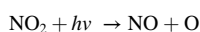
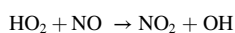
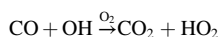
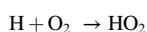
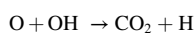
E-mail addresses: teerachai4@gmail.com, teerachai.am@up.ac.th, tum@ucar.edu (T. Amnuaylojaroen).

and NO_x is the key constituent affecting the chemistry of the troposphere (Hagenbjörk et al., 2017). O_3 is considered to be the principal product of tropospheric chemistry. NO_x plays an important role in ozone formation. Specifically, ozone forms as a product of NO_2 photolysis. Then, it is destroyed rapidly in the presence of NO (Seinfeld and Pandis, 1998), as follows:

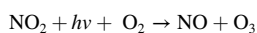
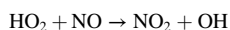
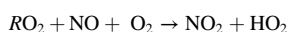
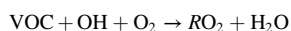


Further, carbon monoxide reacts with the hydroxyl radical, and the hydrogen atom combines very quickly with O_2 to form the hydroperoxyl radical HO_2 . When NO is present, the most important atmospheric reaction that HO_2 undergoes is that with NO . Net formation of O_3 occurs in the reaction because NO is converted to NO_2 by the HO_2 radical rather than by O_3 itself (Seinfeld and Pandis, 1998).

The atmospheric oxidation of CO can be summarized as follows:



In areas of high population, ozone formation can be enhanced by VOC emissions (European Environment Agency, 2008). The photochemical reaction that produces ozone is initiated and maintained by reactive radicals. In the process, other products are formed, such as peroxyacetyl nitrate (PAN), nitric acid, aldehydes, organic acids, particulates, and many short-lived radical species. VOCs act as “fuel” in the ozone formation process, whereas NO functions more or less as a catalyst, because it is regenerated in the formation process. NO also plays a key role in the regeneration of the reactive radicals and the further progress of the reactions. The simplified photochemistry of ozone, which is in reality a complex and highly nonlinear process (European Environment Agency, 2008) is shown below:



NO at high concentrations generally scavenges O_3 , which results in NO_2 formation. Additionally, high NO_2 levels redirect the initial oxidation step of VOCs, preventing net formation of O_3 . Owing to these reactions, if the NO_x concentration decreases, the O_3 concentration can increase in a phenomenon called the VOC-limited regime, where controlling the emission of organic compounds is a more efficient method of reducing the O_3 peak at low VOC/ NO_x ratios. By contrast, meteorological processes can decrease the NO_x concentration more rapidly than the VOC concentration, and consequently the VOC/ NO_x ratio is high. The chemistry tends toward the NO_x -limited case, and NO_x reduction is considered more effective for reducing the peak O_3 concentration (European Environment Agency, 2008). However, Kramp et al. (1994) and

Flocke et al. (1994) indicated that the photochemistry in urban plumes proceeds faster than previously assumed. Oxidation of VOCs contributes to more ozone formation over a shorter time period and to faster removal of NO_x . Hence, a regime in which ozone formation is controlled by the NO_x concentration is reached more quickly than previously thought (Borrell et al., 1995). In addition to the effect on the O_3 peak of emission of its precursor, the meteorological conditions also have an important effect on the O_3 concentration. Liu et al. (1994) suggested that larger temperature increases, a high percentage of low cloud cover, lack of precipitation, clockwise changes in wind direction, and a high percentage of low wind speeds are favorable meteorological conditions contributing to O_3 formation. Under these stagnant conditions, pollutants generally accumulate over the city, in particular over cities located in basins surrounded by mountains. Additionally, the impacts of meteorological conditions on O_3 in Jakarta were studied by Permedi and Oanh (2008). They suggested that the synoptic meteorological conditions such as high-intensity solar radiation, high temperature, and light winds are favorable for peak O_3 concentrations.

In Southeast Asia, fire from biomass burning is an important source that releases the O_3 precursors NO_x and VOCs (Sonkaew and Macatangay, 2015). The peak months of biomass burning in Southeast Asia are typically February and March (Chang and Song, 2010). Biomass burning can have both natural and anthropogenic causes (Yadav and Devi, 2018). Fire emissions also provide an additional atmospheric pathway for ozone production (Chen et al., 2017). Further, fire emissions affect atmospheric chemistry via several processes such as physical and chemical transformations, as well as the dilution and release of chemical oxidants. Photochemistry plays a key role in providing O_3 sinks and sources. The O_3 budget is thus sensitive to the photochemical reactivity of VOCs and NO_x . Under short-term regulatory measures, reduction of anthropogenic VOC emissions is efficient in decreasing O_3 concentrations. However, this approach only changes the VOC- NO_x - O_3 reaction mechanism from NO_x -dependent to VOC-dependent, where VOCs become a limiting factor (Xue et al., 2017). Fire emissions clearly increase the O_3 burden via the resulting photochemistry. As reported by Pfister et al. (2006), who used the chemistry transport Model for Ozone and Related chemical Tracers (MOZART-4) to examine ozone production due to boreal forest fires in Alaska and Canada in summer 2004, revealed that the fire emissions increased the O_3 concentration by approximately 7%–9% over Alaska and 2%–3% over Europe. Furthermore, a study of the tropospheric ozone distribution using the Goddard Earth Observing System (GEOS) Chemistry 3-D global tropospheric chemical transport model with in situ and satellite observations found that decreasing biomass burning emissions can decrease tropospheric ozone by approximately 8% (Parrington et al., 2012). The Transport and Chemical Evolution Over the Pacific campaign, which was conducted during February–April 2001 (Kondo et al., 2004) found that reactive nitrogen (NO_x , PAN, HNO_3 , and nitrate) and O_3 are the main chemical species produced by biomass burning in this region. Further, Amnuaylojaroen et al. (2014) suggested that biomass burning contributes considerably to air pollution in Thailand and Southeast Asia. It makes substantial contributions of 29% and 16% of O_3 and CO , respectively, during the high-emission period in March compared to those in the low-emission period in December. As much as 70% of biomass burning in this region occurs in Myanmar and Laos, as reported by Punsompong and Chantara (2018) and Kiatwattanacharoen et al. (2017).

VOCs are known to be the main contributor to O_3 formation. There are few studies of the role of VOCs in O_3 pollution, in particular few modeling studies. For example, Xue et al. (2017) investigated the distribution and role of VOCs in O_3 formation in the typical industrial city of Baoji in Northwestern China by monitoring the concentrations of related chemical species. They collected air samples at three urban sites. Their results showed that alkenes and aromatics from industry and traffic were the main contributors to the photochemical reactivity. The potential contribution of VOCs to O_3 formation was also studied by Olumayede (2014), who collected data on 16 VOC species from nine sites in an urban

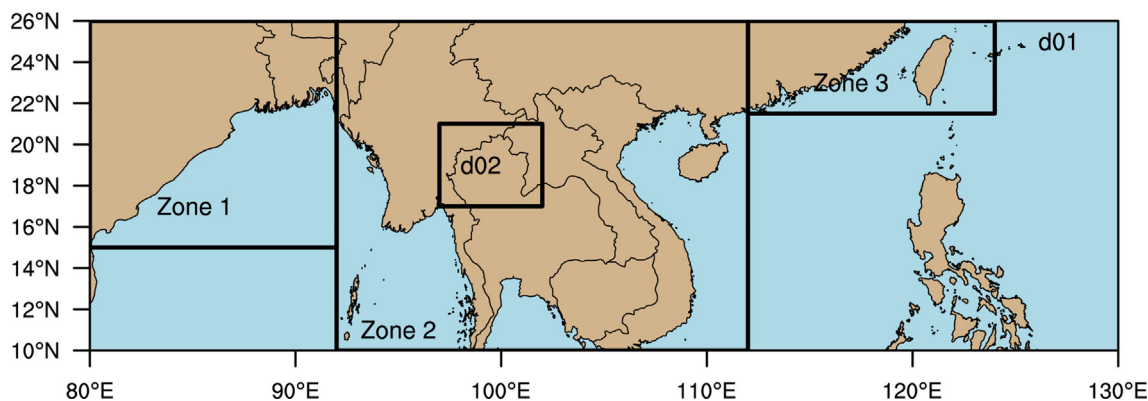


Fig. 1. Study domain and zones used.

settlement of Benin City, Nigeria, using active air sampling. His results revealed that, ranked in terms of the propyl equivalent, alkanes accounted for 58% of the total propyl-equivalent concentrations that contribute to O_3 . A modeling study relating VOCs to O_3 formation was performed by [Ying and Krishnan \(2010\)](#). They modeled the source-oriented SAPRC-99 gas phase photochemical mechanism, which was embedded in the Community Multiscale Air Quality model, to determine the contributions of VOCs to the predicted net O_3 formation from 16 August to 7 September, 2000. The results of their study indicated that VOCs from industrial sources were the main contributor to high O_3 events in Houston–Galveston–Brazoria, Texas.

Owing to the complexity of O_3 formation and quantification of its precursors, it is difficult to control O_3 well. Therefore, in this work, we identified the main VOC ozone precursors from among 10 VOCs in upper Southeast Asia during high-intensity biomass burning episodes (March). Additionally, we also examined the impacts of biomass burning emissions on the relationship between VOCs and O_3 . We used the Weather Research and Forecasting Model with Chemistry (WRF-CHEM) model, version 3.8.1, for two simulations: 1) a control run that included anthropogenic emission, biomass burning emissions, and biogenic emissions and 2) a simulation without biomass burning emissions in March 2014. The paper first describes the model configuration in Section 2 and then describes the data used in this work, such as the input emission data and observations used for model evaluation. Section 3 reports the performance of the model by comparison to several data sets. Finally, the effect of biomass burning emissions on VOCs and its roles in O_3 pollution are analyzed in Section 4. We hope that these findings will provide scientific information that supports the planning of emission reductions.

2. Methodology

2.1. Model configuration

We used the online coupled atmospheric and chemistry model WRF-CHEM, version 3.8.1 ([Grell et al., 2005](#)), to simulate the meteorological conditions and air pollutant concentrations in March 2014. WRF-Chem is a regional air quality model that shares a physical scheme with the WRF model. It has been developed to study several topics in air pollution and atmospheric chemistry research, and it is also used for operational air quality forecasting. In this study, the model was configured with one domain having a horizontal resolution (grid spacing) of 50 km. In addition, the model was set to have 30 vertical levels up to 50 hPa. The outer domain (d01) covers the entire upper mainland of Southeast Asia and some areas of East and South Asia, such as southern China and eastern India, as shown in [Fig. 1](#). This spatial domain was chosen because Southeast Asia is influenced by the East Asian monsoon, which carries air

masses from high latitudes into this region, and by transboundary transport of emissions from countries on the west border, such as Myanmar and Laos, whereas the inner domain (d02), with a horizontal resolution (grid spacing) of 10 km, covers northern Thailand. The WRF-CHEM configurations are shown in [Table 1](#). To resolve water vapor, cloud, and precipitation processes, the model was configured using the Thompson scheme ([Thompson et al., 2004](#)). Here, the subgrid-scale process for solving convection is the Kain–Fritsch scheme ([Kain, 2004](#)). It uses a cloud model with updrafts and downdrafts, and considers the impacts of detrainment and entrainment on cloud formation. The similarity theory scheme was also used to simulate the thermal gradient over the surface, which is responsible for the friction velocities and wind on surfaces ([Paulson, 1970](#); [Dyer and Hicks, 1970](#); [Webb, 1970](#); [Zhang and Anthes, 1982](#)). The planetary boundary layer was configured using the Mellor–Yamada–Janjic scheme ([Janjic, 2002](#)), and the Noah land surface model ([Chen and Dudhia, 2001](#)) was used to represent the heat and moisture fluxes on land. The initial meteorological and boundary conditions were generated from the Final Analysis Data output, which has a $1^\circ \times 1^\circ$ grid spacing and a temporal resolution of 6 h (<https://rda.ucar.edu/datasets/ds083.2/>).

To reduce the effect of the initial conditions, model spin-up was run for February 15–28, 2014. In the WRF-Chem run, the MOZART mechanism was used to represent the gas-phase chemistry ([Emmons et al., 2010](#)). The fast-TUV scheme, which modifies the photolysis rate depending on the presence of clouds and aerosols, was used to calculate the photolysis rate in the model run ([Tie et al., 2003](#)). Further, dry and wet deposition of gases were modeled using the resistance methods of [Wesely \(1989\)](#) and [Neu and Prather \(2012\)](#), respectively. In addition, the Model of Emissions of Gases and Aerosols from Nature (MEGAN) was used to estimate biogenic emissions ([Guenther et al., 2006](#)).

2.2. Emission data

We included both the anthropogenic and biomass burning emission inventories in the simulations. The biomass burning emissions were taken from the Fire INventory (FINN) from the National Center for

Table 1
WRF-Chem configurations.

Scheme	Parameterization
Convection	Kain-Fritsch
Microphysics	Thompson
Planetary Boundary Layer	Mellor–Yamada–Janjic
Land surface model	NOAH
Chemical mechanism	MOZART
Photolysis	Fast-TUV
Deposition	Wesely

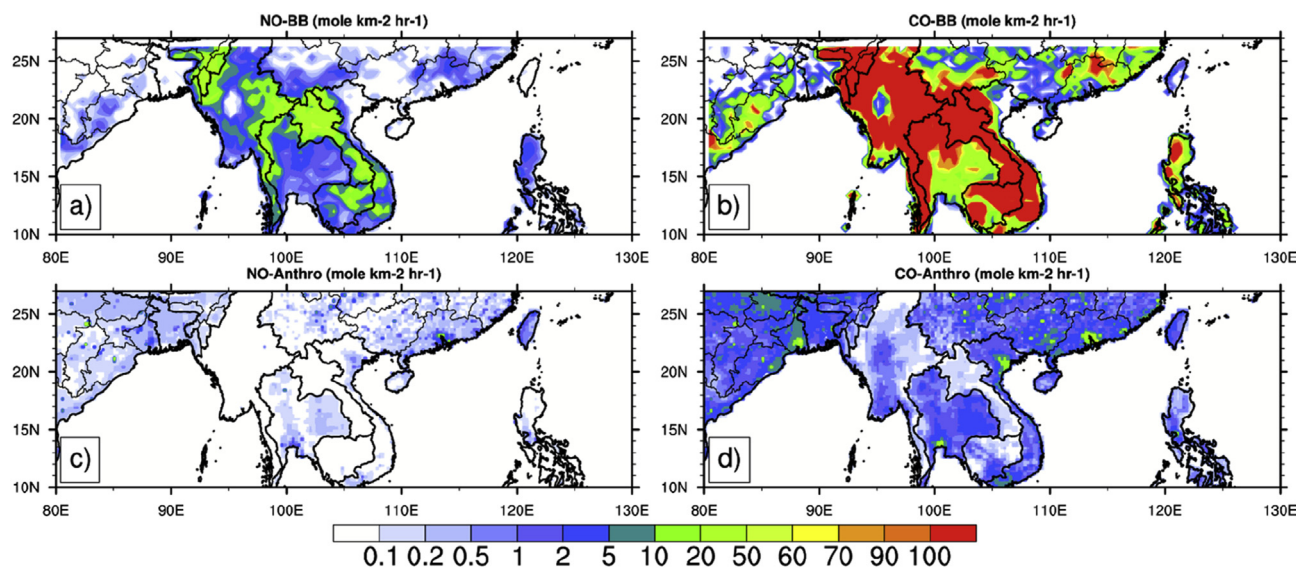


Fig. 2. Monthly average of: a) NO emissions from biomass burning; b) CO emissions from biomass burning; c) NO emissions from anthropogenic emissions; and d) CO emissions from anthropogenic emissions.

Table 2

List of emissions (in units of mole km^2/hr) from different emission sectors in each zone.

Area	Energy		Industry		Residence		Transportation		Biomass	
	CO	NO _x	CO	NO _x	CO	NO _x	CO	NO _x	CO	NO _x
Zone1	0.09	0.08	0.37	0.01	0.79	0.02	0.12	0.06	8.07	0.14
Zone2	0.01	0.02	0.13	0.02	0.57	0.01	0.17	0.03	258.43	5.22
Zone3	0.03	0.13	1.31	0.14	1.09	0.02	0.39	0.11	15.03	0.29

Atmospheric Research (NCAR) following Wiedinmyer et al. (2011). FINN is a global biomass burning emission inventory and provides daily data with 1 km grid resolution. It estimates the trace gas and aerosol emission from any open burning, i.e., wildfires, agricultural fires, biofuel use, and trash burning. The FINN output has global coverage with high temporal and spatial resolution for key chemical species such as formaldehyde and methanol. The biomass burning emissions were also estimated from the MODIS fire and thermal anomalies. Several factors such as the assumed area burned, land cover maps, biomass consumption estimates, and emission factors contribute to the uncertainties in the model simulations.

The Emission Database for Global Atmospheric Research Hemispheric Transport of Air Pollution (EDGAR HTAP) was used to simulate anthropogenic emissions. EDGAR-HTAP provides monthly data on global anthropogenic emissions at a resolution of $0.1^\circ \times 0.1^\circ$. It consists of several chemical components, i.e., CH₄, CO, NO_x, non-methane VOCs, NH₃, SO₂, PM_{2.5}, PM₁₀, organic carbon, and black carbon. Version 2 of EDGAR HTAP includes anthropogenic emissions in several sectors (i.e., international aviation, inland waterways and marine shipping, electricity generation, industrial processes, ground transport, building heating/cooling, equipment, waste disposal or incineration, and agriculture waste burning) (Wiedinmyer et al., 2011; Janssens-Maenhout et al., 2015).

Biogenic emissions were estimated using MEGAN version 2.04 (Guenther et al., 2006). MEGAN is a modeling system that estimates the net emission of isoprene and other trace gases and aerosols produced by the ecosystem into the atmosphere. It is a global model with a base spatial resolution of approximately 1 km². The factors controlling isoprene and other trace gases in MEGAN include biological, physical, and chemical driving variables such as the leaf area index, solar radiation, temperature, and plant functional type.

Fig. 2 shows the average spatial distributions of biomass-based and anthropogenic CO and NO emissions in March. The area was separated into three zones (Fig. 1); zone 1 covers mainly India, zone 2 covers upper

Southeast Asia, and zone 3 covers some areas of southern China. Biomass burning is the main source of CO and NO emissions in March, especially in zone 2, which shows approximately 250 mol/km²/h of CO and 5 mol/km²/h of NO from biomass burning, as shown in Table 2. In addition, zones 1 and 3 also showed high CO and NO emissions from biomass burning, which accounted for approximately 40% of the total emissions in both areas.

2.3. Data used for evaluation

The reanalysis data from the Modern-Era Retrospective Analysis for Research and Applications (MERRA) product was used for model evaluation. The dataset was generated using the GEOS Model Data Assimilation System version 5 for atmospheric data assimilation. This system provides several types of atmospheric data, including precipitation and temperature, with a spatial resolution of $0.5^\circ \times 0.66^\circ$ in a grid with 72 vertical layers at various temporal resolutions, such as hourly, daily, and monthly. Here, we used the monthly data for the 2 m temperature for model evaluation (Rienecker et al., 2011).

The Tropical Rainfall Measuring Mission (TRMM) satellite data used to evaluate the precipitation simulations in this study. It was developed by a joint mission between NASA and the Japan Aerospace Exploration Agency to better understand the distribution and variability of precipitation over the tropics. The TRMM dataset provides hourly, daily, and monthly precipitation data with a spatial resolution of 36 km over the tropical region. The high-resolution precipitation data from TRMM were acquired using the data from its microwave imager, and the data were corrected using surface precipitation gauges (Huffman et al., 1997).

The Ozone Monitoring Instrument (OMI) Level-3 Global Gridded NO₂ data are generally provided by the NASA Goddard Earth Sciences Data and Information Service Center (GES DISC). Its coverage of NO₂ is global and has a spatial resolution of 13 km \times 24 km. The tropospheric NO₂

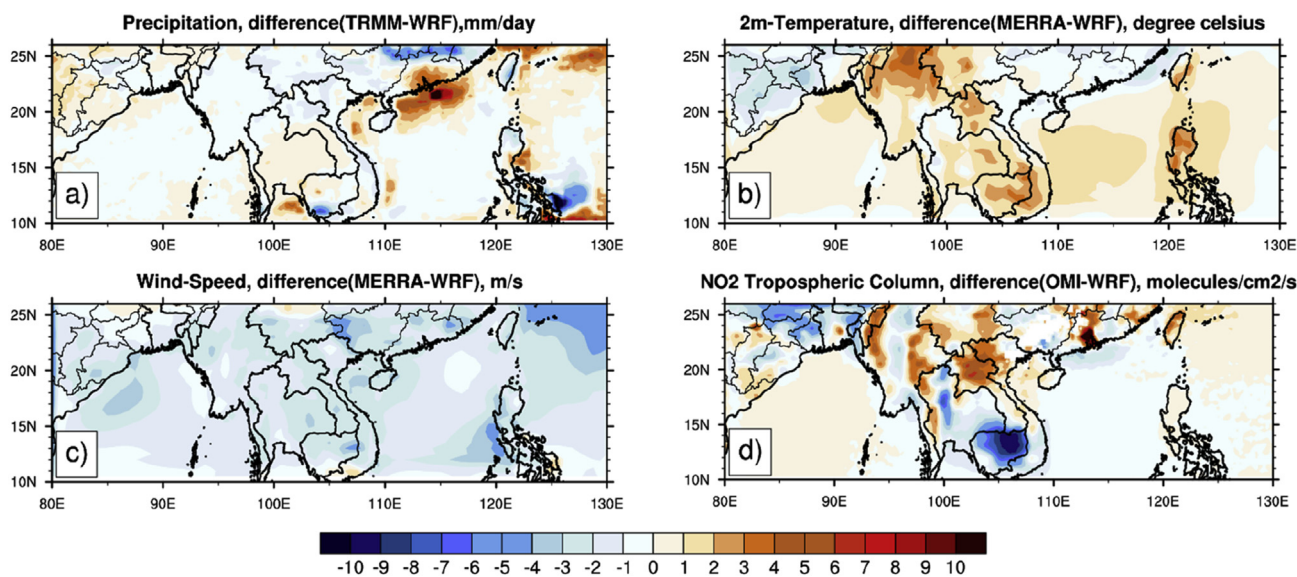


Fig. 3. Difference between the monthly mean of: a) precipitation from TRMM and WRF; b) 2m-temperature from MERRA and WRF; c) wind speed from MERRA and WRF; and d) tropospheric column of NO₂ and WRF-CHEM.

column retrieval algorithm follows Bucseła et al. (2006), who used the differential optical absorption spectroscopy methodology, air mass factors, and typical NO₂ profiles from chemical transport models to obtain the vertical column density. To evaluate the modeled NO₂ profile, we compared the tropospheric NO₂ column from the OMI Level-3 Global Gridded NO₂ data product with WRF-Chem NO₂ columns that were adjusted using the averaging kernel and a priori information provided with the data product (e.g., Emmons et al., 2004; Amnuaylojaroen et al., 2014), as follows:

$$x = Ax + (I - A)x_a \tag{1}$$

where the retrieved mixing ratio is expressed in terms of a linear combination of the real atmospheric profile (x) and a priori information (x_a), balanced according to the averaging kernel A (I is the identity matrix).

From this result, the following was calculated:

$$\text{Mean Bias} = \bar{M} - \bar{O} \tag{2}$$

where \bar{M} is the mean model data, and \bar{O} is the mean observational data. The index of agreement (IOA) is calculated as

$$\text{Index of Agreement, IOA} = 1.0 - \frac{\sum_{i=1}^n (O - M)^2}{\sum_{i=1}^n (|M - \bar{O}| + |O - \bar{O}|)^2} \tag{3}$$

where O is the observational data, M is the model data, and n is the number of model and observational data points. The mean absolute error (MAE) is calculated as

Table 3

Monthly average statistical analysis between the inner domain and ground-based measurement.

Variables	Temperature (°C)	Precipitation (mm/day)	O ₃	NO ₂	CO
Bias	0.39 °C	0.22 mm/day	-0.13 (ppmv)	-0.05 (ppmv)	-0.02 (ppmv)
MAE	0.7 °C	0.26 mm/day	6.5 (ppmv)	2.76 (ppmv)	0.4 (ppmv)
IOA	0.78	0.76	0.57	0.56	0.5

Note: Bias and MAE are in units of ppmv for O₃, NO₂ and CO; IOA is dimensionless.

$$\text{Mean Absolute Error, MAE} = \frac{\sum_{i=1}^n |M - O|}{n} \tag{4}$$

Ground-based measurements in Thailand are made by the Thai Pollution Control Department (PCD). They provide hourly surface concentrations of six chemical species: CO, O₃, SO₂, NO₂, PM₁₀, and PM_{2.5}. Most of the observation instruments use Teledyne Advanced Pollution Instrumentation Model 400 (<http://www.teledyne-api.com/products/400e.asp>) for O₃ and NO₂ and Teledyne Advanced Pollution Instrumentation Model 300 (<http://www.teledyne-api.com/products/300e.asp>) for CO. The O₃ and CO measurements have low detection limits of approximately 0.6 and 40 ppbv, respectively (Amnuaylojaroen et al., 2014).

3. Results & discussion

3.1. Model evaluation

Fig. 3 compares the model precipitation output with the TRMM data (Fig. 1a), the 2 m temperature and wind speed output with the MERRA data (Fig. 1b and c), and the NO₂ tropospheric column with the OMI data (Fig. 1d). The monthly averaged precipitation from the model generally agrees fairly well with the TRMM output in March 2014; however, the precipitation on land was underestimated by approximately 1 mm/day (e.g., Thailand has 1–2 mm/day less precipitation than the TRMM data). The low precipitation is due to the coarse model resolution of 50 km, which makes it difficult to capture the convection process well. As discussed in Amnuaylojaroen et al. (2014), the precipitation in this region is influenced by convection, which is controlled by mesoscale processes. The model generally simulated the temperature moderately well compared to the MERRA data. The WRF model slightly underestimated the temperature over Southeast Asia, especially in Thailand, Myanmar, and Laos, by 1–3 °C. The modeled wind speed exceeds the MERRA data by ~1–2 m/s on land and is ~3–5 m/s higher than the reanalysis output on the South China Sea. The WRF-CHEM output generally underestimated the magnitude of the NO₂ tropospheric column over Southeast Asia by 1×10^{15} to 3×10^{15} molecules/cm²s; however, the model captured the NO₂ tropospheric column well in most areas of Thailand and Myanmar. Some parts of India also showed a lower NO₂ tropospheric column compared to the OMI data. As discussed in Amnuaylojaroen et al. (2014) and Ghude et al. (2013), the model's underestimation of NO₂ was likely affected by

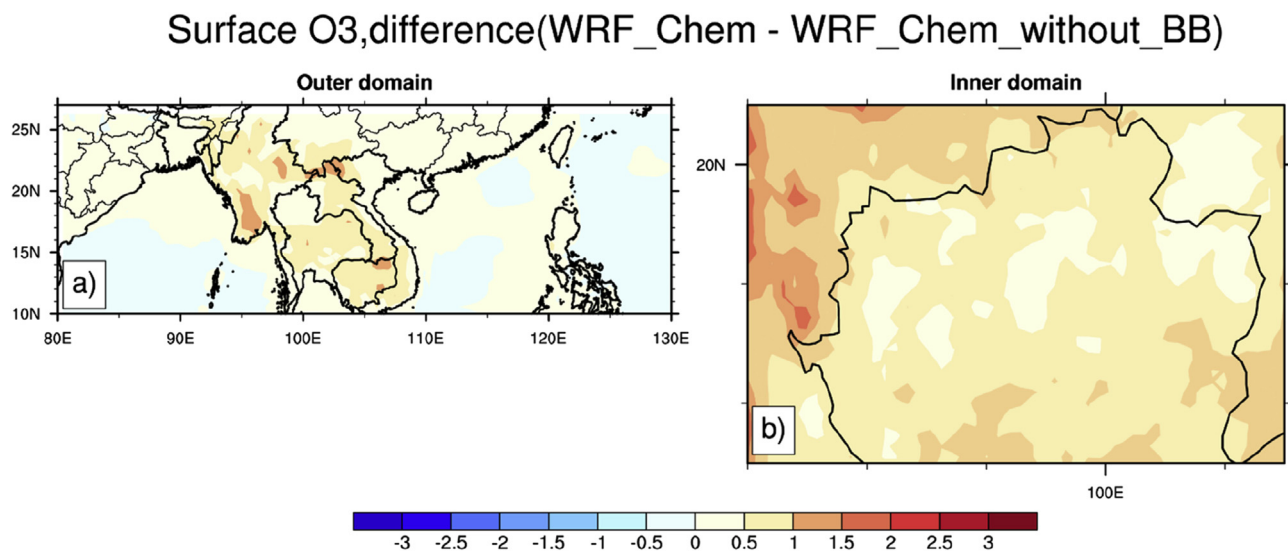


Fig. 4. Difference of surface O₃ (ppmv) between WRF-CHEM simulations including anthropogenic, biomass and biogenic emission and WRF-CHEM simulation excluding biomass burning emission for: a) the outer domain; and b) the inner domain.

the low anthropogenic NO_x emission. Another plausible reason is the error of the model resolution, which must be comparable to or smaller than the spatial variability of NO₂ to accurately model NO₂-OH feedback in the tropospheric NO_x chemistry, as discussed in Martin et al. (2003) and Valin et al. (2011).

The modeled output from the inner domain, i.e., the 2 m temperature, precipitation, NO₂, CO, and O₃ output, was compared to datasets from several types of observation, i.e., satellite, reanalysis data, and ground-based measurement from the Thai PCD, as shown in Table 3. To clarify the model capability, statistical metrics such as the IOA, mean bias, and MAE were used for model evaluation. The WRF-CHEM simulations agree fairly well with the ground-based observations. The monthly mean 2 m temperature and precipitation results are acceptable, with IOAs of 0.78 and 0.76, although the model slightly overpredicted the temperature (by ~0.39 °C) and the precipitation (by ~0.22 mm/day). Overall, most of the chemical species from the model were underestimated compared to the observations. Additionally, WRF-CHEM predicted the chemical species (O₃, NO₂, and CO) moderately well, with IOA values of approximately 0.5. As discussed in Amnuaylojaroen et al. (2014), the aggregated coarse-resolution data for biomass burning emissions are used to calculate all chemical species via the plume rise model in WRF-CHEM. These

calculations may capture much of the thermal buoyancy of fires that lifts these species to high altitudes.

3.2. VOC-NO_x-O₃ system in upper Southeast Asia

In this section, we analyze the role of individual VOCs in O₃ pollution over upper Southeast Asia. The impacts of biomass burning emissions on VOCs, which control the surface O₃, is also examined. Fig. 4 shows the difference between WRF-CHEM simulations including anthropogenic, biomass, and biogenic emissions and WRF-CHEM simulations excluding biomass burning emissions. The biomass burning emissions are responsible for increasing O₃ by approximately 0.5–1.5 ppmv over upper Southeast Asia, whereas they account for an O₃ increase of approximately 0.5 ppmv in some areas of India and southern China. The VOC and NO_x concentrations are generally not directly proportional to the final O₃ concentrations. To control the peak of O₃ formation, the relationships of VOCs and NO_x to O₃ were determined using the indicator species HCHO/NO_y established by Sillman (1995). According to the hydrocarbon-sensitive chemistry in the models, for HCHO/NO_y < 0.28, ozone production is VOC-limited; otherwise, it is said to be NO_x-limited. By examining the ratio of formaldehyde (HCHO) to NO_y (= NO_x + NO₃ +

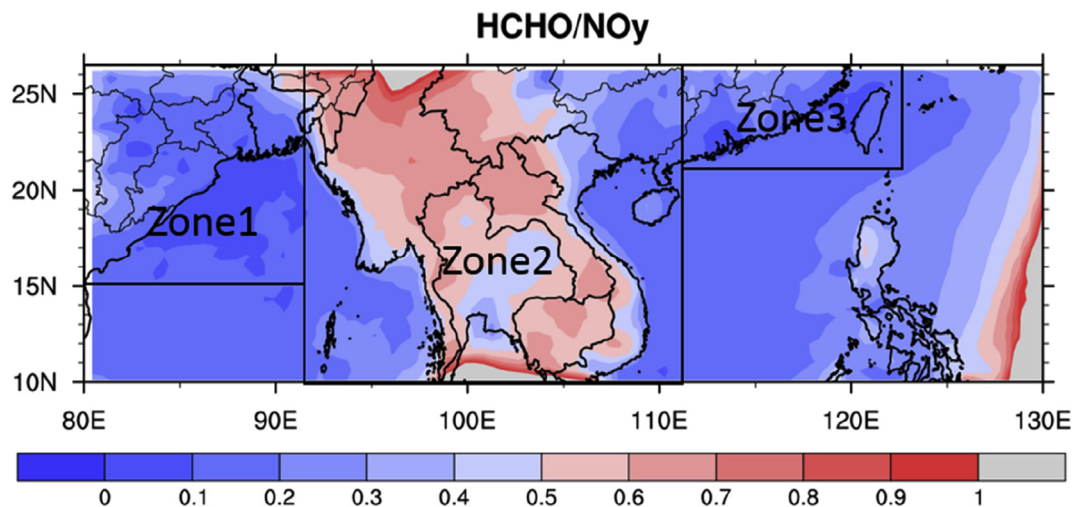


Fig. 5. Ratios of formaldehyde to NO_y (NO_x + NO₃ + N₂O₅ + PAN + HNO₃) in March 2014.

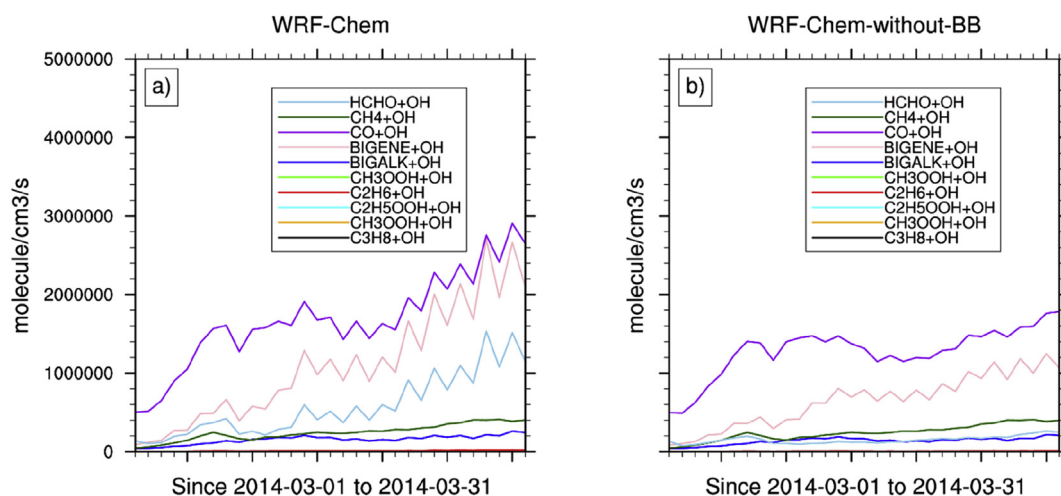


Fig. 6. Average surface peroxy radical production reactions from 9 VOCs and CO for: a) WRF-CHEM; and b) WRF-CHEM without biomass burning emission over zone2.

$\text{N}_2\text{O}_5 + \text{PAN} + \text{HNO}_3$) (Fig. 5), we find that the net O_3 production regime over upper Southeast Asia is clearly NO_x -limited. In NO_x -limited areas, the O_3 concentration is insensitive to both decreases in VOCs at constant NO_x and to the VOC composition.

NO_x generally plays a crucial role in O_3 formation via NO_2 photolysis. Further, O_3 is produced by oxidation of VOCs in the presence of NO_x and sunlight. The effect of VOCs on surface O_3 is analyzed via the radical production reaction rates in Fig. 6. The production of peroxy radicals from OH oxidation of CO and nine VOC chemical species (HCHO, CH_4 , CH_3OOH , C_3H_8 , C_2H_6 , $\text{C}_2\text{H}_5\text{OOH}$, CH_3OOH , BIGENE, and BIGALK) is based on the MOZART-4 mechanism in the WRF-Chem model. These chemical species were analyzed to determine which of them dominate the surface O_3 chemistry. Note that BIGENE and BIGALK represent lumped alkenes and alkanes, whereas the MOZART mechanism uses the name “aldehydes” ($\text{HCHO} = \text{CH}_2\text{O}$) (Emmons et al., 2010). The production of peroxy radicals shows that CO and BIGENE generally dominate the reaction rate by approximately 5×10^5 – 3×10^6 molecules/ cm^3/s and 1×10^5 – 2.5×10^6 molecules/ cm^3/s , respectively. These results show that CO and BIGENE are the main VOCs contributing to surface O_3 formation by atmospheric oxidation in upper Southeast Asia. Additionally, biomass burning emissions increase both the CO and BIGENE reaction rates to approximately 0.5×10^6 and 1×10^6 molecules/ cm^3/s , respectively. These results show that biomass burning emissions potentially contribute greatly to CO and BIGENE, which control surface O_3 formation in upper Southeast Asia.

4. Conclusion

We first applied a regional atmospheric chemistry model to study the effect of VOCs on surface O_3 formation in upper Southeast Asia during an intense biomass burning episode. The model can be used to analyze the contributions of VOCs to surface O_3 formation with acceptable accuracy. By comparing the model results to TRMM, MERRA, and OMI datasets, we found that the model generally agrees well with the precipitation, 2 m temperature, and wind data. However, the magnitude of the NO_2 tropospheric column is generally underestimated in most areas of upper Southeast Asia. A comparison of WRF-CHEM simulations with and without biomass burning indicated that biomass burning emissions are responsible for increasing O_3 by approximately 1 ppmv in upper Southeast Asia. However, the underestimation of the modeled NO_2 tropospheric column likely affected the surface O_3 simulation in the model, especially because this region is NO_x -limited. If the underestimation of NO_2 is corrected, the model would probably simulate the surface O_3 concentrations more accurately, which might increase the surface O_3

difference. An analysis of the surface peroxy radical production reactions of nine VOCs and CO showed that CO and BIGENE are the two main chemical species that produce O_3 by atmospheric oxidation in upper Southeast Asia. We also found that biomass burning emissions play a key role by increasing both the CO and BIGENE reaction rates and thus tend to increase the production of O_3 in upper Southeast Asia.

Declarations

Author contribution statement

Teerachai Amnuaylojaroen: Conceived and designed the experiments; Performed the experiments; Analyzed and interpreted the data; Contributed reagents, materials, analysis tools or data; Wrote the paper.

Ronald C. Macatangay: Analyzed and interpreted the data; Wrote the paper.

Suratsawadee Khodmanee: Contributed reagents, materials, analysis tools or data.

Funding statement

This work was supported by the National Astronomical Research Institute of Thailand (NARIT).

Competing interest statement

The authors declare no conflict of interest.

Additional information

No additional information is available for this paper.

Acknowledgements

We acknowledge the Global Modelling and Assimilation Office (GMAO) and the GES DISC for the dissemination of MERRA and TRMM data. We also acknowledge the use of the WRF-Chem preprocessor tool {mozbc, fire_emiss, bio_emiss, anthro_emiss} provided by the Atmospheric Chemistry Observations and Modeling (ACOM) lab of NCAR. Finally, we greatly appreciate the scientific suggestions on the manuscript made by Mary Barth (NCAR).

References

- Amnuaylojaroen, T., Barth, M.C., Emmons, L.K., Carmichael, G.R., Kreasuwun, J., Prasitwattanaseree, S., Chantara, S., 2014. Effect of different emission inventories on ozone and carbon monoxide in Southeast Asia. *Atmos. Chem. Phys.* 14, 12983–13012.
- Amnuaylojaroen, T., Barth, M.C., Pfister, G.G., Bruyere, C.C., 2018. Simulation of emissions, air quality, and climate contribution in Southeast Asia for March and December. In: Vadrevu, K., Ohara, T., Justice, C. (Eds.), *Land-Atmospheric Research Applications in South and Southeast Asia*, Springer Remote Sensing/Photogrammetry. Springer, Cham, pp. 233–254.
- Bell, M.L., Dominici, F., 2008. Effect modification by community characteristics on the short-term effects of ozone exposure and mortality in 98 US communities. *Am. J. Epidemiol.* 167 (8), 986–997.
- Bell, M.L., McDermott, A., Zeger, S.L., Samet, J.M., Dominici, F., 2004. Ozone and short-term mortality in 95 U.S. Urban communities 1987–2000. *J. Am. Med. Assoc.* 292 (19), 2372–2378.
- Borrell, P., Buitjes, P., Grennfelt, P., Hov, Æ., van Aalst, R., Fowler, D., Megie, G., Moussiopoulos, N., Warneck, P., Volz-Thomas, A., Wayne, R., 1995. Photo-oxidants, Acidification and Tools; Policy Applications of EUROTRAC Results, EUROTRAC ISS, Garmisch-Partenkirchen, Germany.
- Bucsel, E.J., Celarier, E.A., Wening, M.O., Gleason, J.F., Veefkind, J.P., Boersma, K.F., Brinksma, E.J., 2006. Algorithm for NO₂ vertical column retrieval from the ozone monitoring instrument. *IEEE T. Geosci. Remote* 44, 1245–1258.
- Chang, d., Song, Y., 2010. Estimates of biomass burning emissions in tropical Asia based on satellite-derived data. *Atmos. Chem. Phys.* 10, 2335–2351.
- Chen, F., Dudhia, J., 2001. Coupling an advanced landsurface/hydrology model with the Penn State/NCAR MM5 modeling system, Part 1: model description and implementation. *Mon. Weather Rev.* 129, 569–585.
- Chen, et al., 2017. A review of biomass burning: emissions and impacts on air quality, health and climate in China. *Sci. Total Environ.* 579, 1000–1034.
- Dyer, A.J., Hicks, B.B., 1970. Flux-gradient relationships in the constant flux layer. *Quart. J. Roy. Meteor. Soc.* 96, 715–721.
- Ebi, K.L., McGregor, G., 2008. Climate change, tropospheric ozone and particulate matter, and health impacts. *Environ. Health Perspect.* 116 (11), 1449–1455.
- Emmons, L.K., et al., 2004. Validation of Measurements of Pollution in the Troposphere (MOPITT) CO retrievals with aircraft in situ profiles. *J. Geophys. Res.* 109, D03309.
- Emmons, L.K., et al., 2010. Description and evaluation of the model for ozone and related chemical Tracers, version 4 (MOZART-4). *Geosci. Model Dev. (GMD)* 3, 43–67.
- European Environment Agency, 2008. Tropospheric ozone: background information. In: *Tropospheric Ozone in EU - The Consolidated Report*.
- Felzer, B.S., Cronin, T., Reilly, J.M., Melillo, J.M., Wang, X., 2007. Impacts of ozone on trees and crops. *Compt. Rendus Geosci.* 339 (11–12), 784–897.
- Flocke, F., Volz-Thomas, A., Kley, D., 1994. The use of alkyl nitrate measurements for the characterization of the ozone balance at TOR-station no. 11, Schauinsland, A contribution to subproject TOR. In: Borrell, P., Borrell, P.M., Seiler, W. (Eds.), *Transport and Transformation of Pollutants in the Troposphere*, Proceedings of EUROTRAC Symposium '94. SPB Academic Publishing, The Hague, the Netherlands.
- Ghude, S.D., Pfister, G.G., Chinmay, J., Vander, A.R.J., Emmons, L.K., Kumar, R., 2013. Satellite constraints of nitrogen oxide (NO_x) emissions from India based on OMI observations and WRF-Chem simulations. *Geophys. Res. Lett.* 40, 423–428.
- Grell, G.A., Peckham, S.E., Schmitz, R., McKeen, S.A., Frost, G., Skamarock, W.C., Eder, B., 2005. Fully coupled “online” chemistry within the WRF model. *Atmos. Environ.* 29, 6957–6975.
- Guenther, A., Karl, T., Harley, P., Wiedinmyer, C., Palmer, P.I., Geron, C., 2006. Estimates of global terrestrial isoprene emissions using MEGAN (model of emissions of gases and aerosols from nature). *Atmos. Chem. Phys.* 6, 3181–3210.
- Hagenbjörk, A., Malmqvist, E., Mattisson, K., Sommar, N.J., Modig, L., 2017. The spatial variation of O₃, NO, NO₂ and NO_x and the relation between them in two Swedish cities. *Environ. Monit. Assess.* 189 (4), 161.
- Huffman, Coauthors, 1997. The global precipitation climatology project (GPCP) combined precipitation dataset. *Bull. Am. Meteorol. Soc.* 78, 5–20.
- Janjic, Z.I., 2002. Nonsingular Implementation of the Mellor–Yamada Level 2.5 Scheme in the NCEP Meso Model, National Oceanic and Atmospheric Administration Science Center, Camp Springs, MD, NCEP Office Note, No. 437, p. 61.
- Janssens-Maenhout, G., et al., 2015. HTAP_v2.2: a mosaic of regional and global emission grid maps for 2008 and 2010 to study hemispheric transport of air pollution. *Atmos. Chem. Phys.* 15, 11411–11432.
- Kain, J.S., 2004. The Kain-Fritsch convective parameterization: an update. *J. Appl. Meteorol.* 43, 170–181.
- Kiatwattananacharoen, S., Prapamontol, T., Singharat, S., Chantara, S., Thavorniyutikarn, P., 2017. Exploring the sources of PM₁₀ burning-season Haze in northern Thailand using nuclear analytical techniques. *CMU J. Nat. Sci.* 16 (4), 307–325.
- Kondo, Y., et al., 2004. Impacts of biomass burning in Southeast Asia on ozone and reactive nitrogen over the western Pacific in spring. *J. Geophys. Res.* 109.
- Kramp, F., Buers, H.J., Flocke, F., Klemp, D., Kley, D., Pätz, H.W., Schmitz, T., Volz-Thomas, A., 1994. Determination of OH-concentrations from the decay of C₅-C₈ hydrocarbons between Freiburg and Schauinsland: implications on the budgets of olefins, a contribution to subproject TOR. In: Borrell, P., Borrell, P.M., Seiler, W. (Eds.), *Transport and Transformation of Pollutants in the Troposphere*, Proceedings of EUROTRAC Symposium '94. SPB Academic publishing, The Hague, the Netherlands.
- Lelieveld, J., Barlas, C., Giannadaki, D., Pozzer, A., 2013. Model calculated global, regional and megacity premature mortality due to air pollution. *Atmos. Chem. Phys.* 13, 7023–7037.
- Lenka, S., Lenka, N.K., 2012. Impact of tropospheric ozone on agroecosystem: an assessment. *J. Agric. Phys.* 12 (1), 1–11.
- Liu, C.-M., Huang, C.-Y., Shieh, S.-L., Wu, C.-C., 1994. Important meteorological parameters for ozone episodes experienced in the Taipei basin. *Atmos. Environ.* 28 (1), 159–173.
- Martin, R.V., Jacob, D.J., Chance, K., Kurosu, T.P., Palmer, P.I., Evans, M.J., 2003. Global inventory of nitrogen oxide emissions constrained by space-based observations of NO₂ columns. *J. Geophys. Res.* 108 (D17), 4537–4548.
- Melkonyan, A., Kuttler, W., 2012. Long-term analysis of NO, NO₂ and O₃ concentrations in North Rhine-Westphalia, Germany. *Atmos. Environ.* 60, 316–326.
- Neu, J.L., Prather, M.J., 2012. Toward a more physical representation of precipitation scavenging in global chemistry models: cloud overlap and ice physics and their impact on tropospheric ozone. *Atmos. Chem. Phys.* 12, 3289–3310.
- Nuvolone, D., Petri, D., Voller, F., 2018. The effect of ozone on human health. *Environ. Sci. Pollut. Res.* 25 (9), 8074–8088.
- Olumayede, E.G., 2014. Atmospheric volatile organic compounds and ozone creation potential in an urban center of southern Nigeria. *Int. J. Atmos. Sci.* 7. Article ID 764948.
- Parrington, M., et al., 2012. The influence of boreal biomass burning emissions on the distribution of tropospheric ozone over North America and the North Atlantic during 2010. *Atmos. Chem. Phys.* 12, 2077–2098.
- Paulson, C.A., 1970. The mathematical representation of wind speed and temperature profiles in the unstable atmospheric surface layer. *J. Appl. Meteorol.* 9, 857–861.
- Permadi, D.A., Oanh, N.T.K., 2008. Episodic ozone air quality in Jakarta in relation to meteorological conditions. *Atmos. Environ.* 42, 6806–6815.
- Pfister, G.G., et al., 2006. Ozone production from the 2004 North American boreal fires. *J. Geophys. Res.* 111, D24S07.
- Punsompong, P., Chantara, S., 2018. Identification of potential sources of PM₁₀ pollution from biomass burning in northern Thailand using statistical analysis of trajectories. *Atmos. Pollut. Res.* 9 (6), 1038–1051.
- Rienecker, M.M., et al., 2011. MERRA – NASA’s Modern-Era retrospective analysis for research and Applications. *J. Clim.* 24, 3624–3648.
- Seinfeld, H.J., Pandis, S.N., 1998. *Atmospheric Chemistry and Physics from Air Pollution to Climate Change*. John Wiley and Sons, INC.
- Sillman, 1995. The use of NO_y, H₂O₂, and HNO₃ as indicators for ozone-NO_x-hydrocarbon sensitivity in urban locations. *J. Geophys. Res.*
- Sonkaew, T., Macatangay, R., 2015. Determining relationships and mechanisms between tropospheric ozone column concentrations and tropical biomass burning in Thailand and its surrounding regions, 10 (6), 065009.
- Thompson, G., Rasmussen, R.M., Manning, K., 2004. Explicit forecasts of winter precipitation using an improved bulk microphysics scheme, Part 1: description and sensitivity analysis. *Mon. Weather Rev.* 132, 519–542.
- Tie, X., Madronich, S., Walters, S., Zhang, R., Rasch, P., Collins, W., 2003. Effects of clouds on photolysis and oxidants in the troposphere. *J. Geophys. Res.* 108, 4642.
- Valin, L.C., Russell, A.R., Hudman, R.C., Cohen, R.C., 2011. Effects of model resolution on the interpretation of satellite NO₂ observations. *Atmos. Chem. Phys.* 11, 11647–11655.
- Webb, E.K., 1970. Profile relationships: the log-linear range, and extension to strong stability. *Quart. J. Roy. Meteor. Soc.* 96, 67–90.
- Wesely, M.L., 1989. Parameterization of surface resistance to gaseous dry deposition in regional numerical models. *Atmos. Environ.* 16, 1293–1304.
- Wiedinmyer, C., Akagi, S.K., Yokelson, R.J., Emmons, L.K., AlSaadi, J.A., Orlando, J.J., Soja, A.J., 2011. The Fire Inventory from NCAR (FINN): a high resolution global model to estimate the emissions from open burning. *Geosci. Model Dev. (GMD)* 4, 625–641.
- Xue, Y., Ho, S.S.H., Huang, Y., Li, B., Wang, L., Dai, W., Lee, S., 2017. Source apportionment of VOCs and their impacts on surface ozone in an industry city of Baoji, Northwestern China. *Nature* 7, 9979.
- Yadav, I.C., Devi, N.L., 2018. Biomass burning. *Regional Air Qual. Clim. Change*.
- Ying, Q., Krishnan, A., 2010. Source contributions of volatile organic compounds to ozone formation in southeast Texas, 115 (D17306).
- Zhang, D.-L., Anthes, R.A., 1982. A high-resolution model of the planetary boundary layer—sensitivity tests and comparisons with SESAME-79 data. *J. Appl. Meteorol.* 21, 1594–1609.